EPJ Plus

EPJ.org
your physics journal

Eur. Phys. J. Plus (2018) **133**: 173 DOI 10.1140/epjp/i2018-11999-6

Exact solutions of the Navier-Stokes equations generalized for flow in porous media

Edoardo Daly, Hossein Basser and Murray Rudman

Società Italiana di Fisica

Springer

Eur. Phys. J. Plus (2018) **133**: 173
DOI 10.1140/epjp/i2018-11999-6

THE EUROPEAN PHYSICAL JOURNAL PLUS

Regular Article

Exact solutions of the Navier-Stokes equations generalized for flow in porous media

Edoardo Daly[1,a], Hossein Basser[1], and Murray Rudman[2]

[1] Department of Civil Engineering, Monash University, Clayton, VIC, Melbourne, Australia
[2] Department of Mechanical and Aerospace Engineering, Monash University, Clayton, VIC, Melbourne, Australia

Received: 4 December 2017 / Revised: 24 March 2018
Published online: 4 May 2018 –

Abstract. Flow of Newtonian fluids in porous media is often modelled using a generalized version of the full non-linear Navier-Stokes equations that include additional terms describing the resistance to flow due to the porous matrix. Because this formulation is becoming increasingly popular in numerical models, exact solutions are required as a benchmark of numerical codes. The contribution of this study is to provide a number of non-trivial exact solutions of the generalized form of the Navier-Stokes equations for parallel flow in porous media. Steady-state solutions are derived in the case of flows in a medium with constant permeability along the main direction of flow and a constant cross-stream velocity in the case of both linear and non-linear drag. Solutions are also presented for cases in which the permeability changes in the direction normal to the main flow. An unsteady solution for a flow with velocity driven by a time-periodic pressure gradient is also derived. These solutions form a basis for validating computational models across a wide range of Reynolds and Darcy numbers.

1 Introduction

The study of fluid flow in porous media attracts attention because of its occurrence in many natural systems and the large number of applications in engineering and the physical sciences, such as groundwater movement [1, 2] and heat and mass transfer in composite media [3].

The most commonly used model for momentum transfer in flows of Newtonian fluids in porous media is the Darcy equation, which states that the velocity of the fluid is proportional to the head gradient [1]. When combined with the continuity equation, exact solutions of mathematical models for flow in porous media using Darcy's law are available for many practical applications. In studies of groundwater flow, for example, analytical solutions of steady flow results in a linear Laplace equation [2]. For unsteady flow, solutions in unconfined aquifers are often obtained by employing the Dupuit approximation [1], which neglects streamline curvature; in this case, the equations can be written in a form equivalent to the shallow water equations for open channel flow, and continuity and momentum can be combined, leading to a non-linear diffusion equation. This non-linear equation is often referred to as the Boussinesq equation [2]. Solutions of the linearized Boussinesq equation are available in the literature in groundwater hydrology [2, 4, 5], with some solutions of the non-linear Boussinesq equation also available (see, *e.g.* [6–8] and references therein).

Several variations of Darcy's law have been developed to account for a range of different phenomena arising in various problems. These led to the development of alternative momentum equations with various degrees of complexity [3, 9]. The so-called Forchheimer's equation, for example, introduces an additional inertial drag term in the momentum equation proportional to the square of the velocity, while the equation commonly known as Brinkman equation accounts for the resistance to the flow as in Darcy's and includes a term associated with the viscosity of the fluid [10].

Because the Brinkman equation reduces to the Navier-Stokes momentum equation when the permeability tends to infinity and the porosity of the medium equals one, this model has been largely applied to flows adjacent to porous media [11, 12]. Interestingly, use of the Navier-Stokes equations with additional terms related to the resistance that porous media exert on the flow is becoming more common in the literature as use of the Smoothed Particle Hydrodynamics (SPH) technique is increasingly being applied to porous media problems [13–15]. SPH is a meshless

[a] e-mail: edoardo.daly@monash.edu

Lagrangian numerical method often employed for the solution of the Navier-Stokes equations [16], in which the non-linear terms in the equations are simply handled by the advection of the computational nodes (*i.e.*, the SPH particles). Therefore, the method automatically includes the non-linear terms in the equations. In the context of SPH modelling, various existing numerical schemes often adopt *ad hoc* approximations to represent different terms in the equations that are being solved. Solutions are often compared to data from experiments, because analytical solutions of the Navier-Stokes equations are limited to only a few cases [17–19]. Exact solutions of the Navier-Stokes equations generalized to describe flow in porous media using the Brinkman equation are even less common and mainly belong to the mathematical literature [9, 20, 21].

The aim of this study is to derive and present a number of solutions of the Navier-Stokes equations applied to porous media flow that can be used as a benchmark for numerical simulations. The solutions presented here all refer to two-dimensional problems with parallel flow for cases with both constant and spatially variable permeability along the main flow direction, including steady and unsteady solutions.

2 Governing equations

The focus is on two-dimensional problems; accordingly, the Navier-Stokes equations in Cartesian coordinates for an incompressible fluid flowing in a porous medium can be written as [15]

$$\frac{\partial u}{\partial x} + \frac{\partial v}{\partial y} = 0, \tag{1}$$

$$\frac{Du}{Dt} = \frac{\partial u}{\partial t} + u\frac{\partial u}{\partial x} + v\frac{\partial u}{\partial y} = -\frac{\epsilon}{\rho}\frac{\partial p}{\partial x} + \frac{\mu}{\rho}\left(\frac{\partial^2 u}{\partial x^2} + \frac{\partial^2 u}{\partial y^2}\right) + \epsilon g_x - R_x, \tag{2}$$

$$\frac{Dv}{Dt} = \frac{\partial v}{\partial t} + u\frac{\partial v}{\partial x} + v\frac{\partial v}{\partial y} = -\frac{\epsilon}{\rho}\frac{\partial p}{\partial y} + \frac{\mu}{\rho}\left(\frac{\partial^2 v}{\partial x^2} + \frac{\partial^2 v}{\partial y^2}\right) + \epsilon g_y - R_y, \tag{3}$$

where eq. (1) is the continuity equation and eqs. (2) and (3) are the momentum equations along the two directions x and y. In eqs. (1)–(3), $D(\cdot)/Dt$ indicates the material derivative, t being time, u and v are the components of the Darcy velocity, $\mathbf{u}$, along the directions x and y, p is pressure, ρ and μ are the fluid density and dynamic viscosity, g_x and g_y are the components of the gravity vector, $\mathbf{g}$, along x and y, and ϵ is porosity. The components of the velocity of the fluid can be calculated as $u_f = u/\epsilon$ and $v_f = v/\epsilon$. Although Brinkman suggested that the viscosity in the diffusive term (*i.e.*, $\mu\nabla^2\mathbf{u}$) of the equations might be different from the actual viscosity of the fluid [10], this difference will not be taken into account here, because it does not appear to have an appreciable effect in numerical models used to reproduce experimental results [11, 22, 23]. The last terms in eqs. (2) and (3), R_x and R_y, describe the resistance to the flow due to the porous medium provided the coordinate axes are aligned with the principal directions, such that the permeability tensor is diagonal. These drag terms depend on the porous medium properties and the velocity of the fluid, and they can be expressed in general as [3, 15]

$$\begin{aligned} R_x &= \frac{\mu\epsilon}{\rho\kappa_x}u + \frac{\epsilon\rho c_F}{\mu\sqrt{\kappa_x}}u|u| \\ R_y &= \frac{\mu\epsilon}{\rho\kappa_y}v + \frac{\epsilon\rho c_F}{\mu\sqrt{\kappa_y}}v|v|, \end{aligned} \tag{4}$$

where κ_x and κ_y are the permeability of the medium along the directions x and y, and c_F is the Forchheimer coefficient. The linear term is dominant for flows with low pore-scale Reynolds numbers, while the quadratic term becomes important as the pore-scale Reynolds number increases [3, 24]. When $\epsilon = 1$ and both κ_x and κ_y tend to infinity, eqs. (1)–(3) become the classical form of the Navier-Stokes equations for laminar flow of Newtonian fluids.

3 Exact solutions

In the remainder of the paper some exact solutions of eqs. (1)–(3) are derived and presented for cases in which the flow occurs with straight and parallel streamlines, although these do not need to be aligned with the coordinate axes. These solutions are all for the case of porous media where the porosity ϵ does not change in either time or space. When considering media with varying porosity, the velocities in different media are affected, thereby introducing complications in the definition of the conditions at the interfaces where ϵ changes [11, 12, 25]. The proper definition of these conditions is still matter of debate and will not be addressed here.

The solutions derived here refer to either steady-state flow conditions or flows driven by a time-periodic external forcing. All cases assume that the permeability does not vary in the x-direction, and both κ_x and κ_y are function of y only.

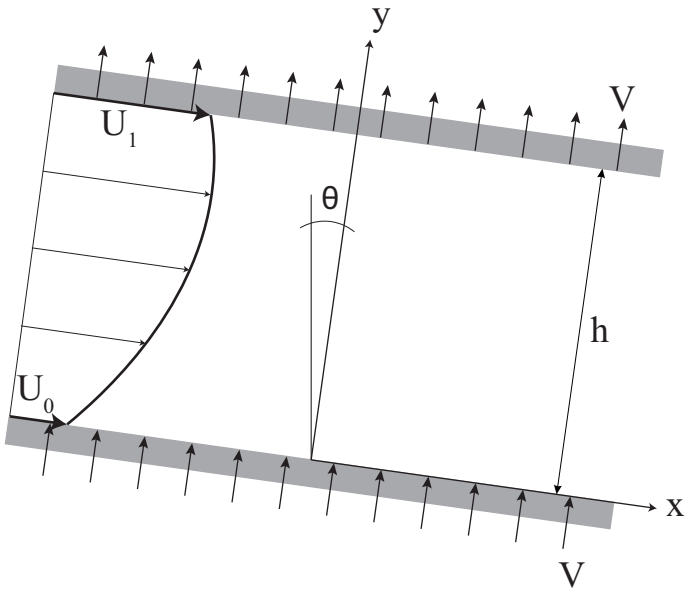

Fig. 1. Geometry of parallel flow between permeable boundaries.

3.1 Constant permeability κ_x and linear drag

A flow bounded between plane parallel (permeable) boundaries is considered (fig. 1). It is assumed that the flow is in steady state and that boundaries are aligned in the x-direction; thus, the y-direction is perpendicular to the boundaries that are positioned at $y = 0$ and $y = h$. If the flow in the x-direction is driven by gravity and a constant pressure gradient in x (*i.e.*, $\partial_x p = -\Delta P$), the velocity will be homogeneous in x and $u = u(y)$. The drag is assumed to be linear in u, such that $c_F = 0$ in eq. (4).

Assuming that the fluid at the boundaries can have an externally imposed (constant) velocity at $y = 0$ and $y = h$, the boundary conditions for the problem are

$$\begin{aligned} u(0) &= U_0 \quad \text{and} \quad v(0) = V, \\ u(h) &= U_1 \quad \text{and} \quad v(h) = V, \end{aligned} \tag{5}$$

where U_0 and U_1 are the constant velocities of the fluid at the two boundaries. Because the boundaries are assumed to be permeable, fluid can be injected through one boundary with a y–velocity of V. Given that $u = u(y)$, according to eq. (1) $\partial_x u = -\partial_y v = 0$; therefore, v remains constant across the medium, *i.e.*, $v = V$ everywhere, including at $y = h$. The system of eqs. (1)–(3) thus becomes

$$\frac{\mathrm{d}^2 u}{\mathrm{d}y^2} - \frac{\rho V}{\mu}\frac{\mathrm{d}u}{\mathrm{d}y} - \frac{\epsilon}{\kappa_x}u = -\frac{\epsilon}{\mu}(\Delta P + \rho g_x), \tag{6}$$

$$\frac{\partial p}{\partial y} = \rho g_y - \frac{\mu}{\kappa_y}V. \tag{7}$$

Equation (7) results in a pressure profile that changes along y. Accounting for all the assumptions made, p can be written as [20]

$$\begin{aligned} p &= -\Delta P x + \rho g_y y - \frac{\rho}{\epsilon}\int_y R_y(\zeta)\mathrm{d}\zeta + f(t) \\ &= -\Delta P x + \rho g_y y - V\mu \int_y \frac{\mathrm{d}\zeta}{\kappa_y(\zeta)} + f(t), \end{aligned} \tag{8}$$

where ζ is a dummy variable of integration and $f(t)$ is a generic function of time. Equation (7) is independent of eq. (6), which is thus the equation that remains to be solved. Because g_y and κ_y do not affect the dynamics of u, and in the cases analyzed the gradient of pressure along x will be assumed constant, p will have in all cases presented here a form similar to eq. (8). In the remaining of the paper, the focus will be on the velocity profile $u(y)$ and, therefore, the expression of p in the following cases will not be explicitly given.

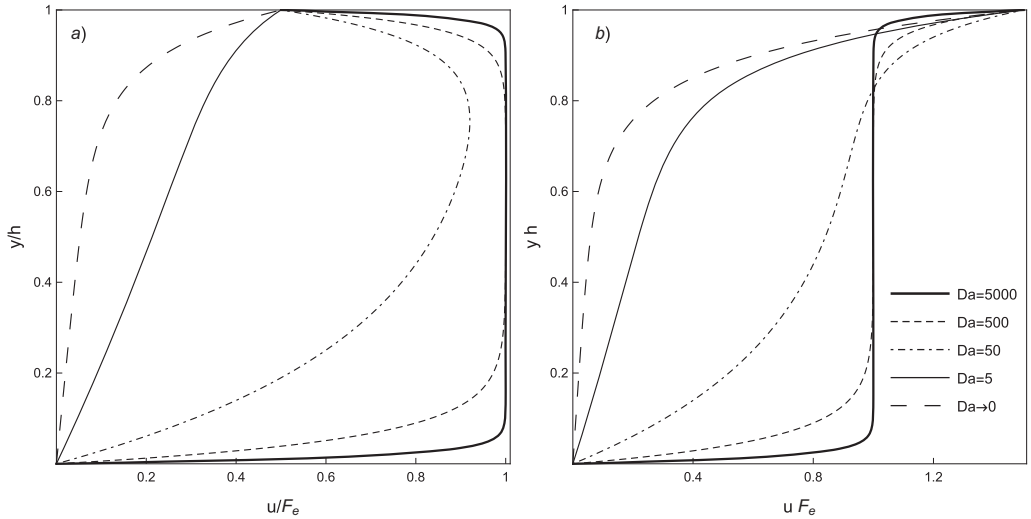

Fig. 2. Examples of velocity profiles for different values of Da as a function of $\tilde{y} = y/h$ for a straight parallel flow (eq. (9)), with (a) $U_1 = F_e/2$ and (b) $U_1 = 1.5\,F_e$, F_e being $\kappa_x(P + \rho g_x)/\mu$ ($F_e = F_{eh} = h^2(P + \rho g_x)/\mu$ in the absence of a porous medium, when $\kappa_x \to \infty$ and $\epsilon = 1$). Other parameters are $Re = 10$ and $U_0 = 0$.

A general solution of eq. (6) for the boundary conditions in eq. (5) can be found as (appendix A)

$$u(y) = F_e \left[1 + \left(\frac{U_0}{F_e} - 1\right) e^{Re\,\tilde{y}/2} \frac{\sinh(\sqrt{\alpha}(1-\tilde{y}))}{\sinh(\sqrt{\alpha})} + \left(\frac{U_1}{F_e} - 1\right) e^{-Re(1-\tilde{y})/2} \frac{\sinh(\sqrt{\alpha}\tilde{y})}{\sinh(\sqrt{\alpha})}\right], \tag{9}$$

where $F_e = \kappa_x(\Delta P + \rho g_x)/\mu$, $\tilde{y} = y/h$, $\alpha = Re^2/4 + Da$, with $Re = \rho V h/\mu$ and $Da = h^2\epsilon/\kappa_x$ being forms of Reynolds and Darcy numbers. Note that Re can be positive or negative depending on the sign of V [17]. Moreover, the Darcy number is here written differently from its more common definition (*i.e.*, κ_x/h^2) to simplify the expressions of the solutions that are later presented.

The solution in eq. (9) can be compared to the velocity profile in the absence of porous media. Assuming $\epsilon = 1$ and $\kappa_x \to \infty$ (*i.e.*, $Da \to 0$), the term $-\epsilon u/\kappa$ in eq. (6) disappears, and the velocity profile for the Navier-Stokes equations without a porous medium becomes

$$u = \frac{F_{eh}}{Re}\tilde{y} + U_0 \frac{e^{Re\,\tilde{y}} - e^{Re}}{1 - e^{Re}} + \left(U_1 - \frac{F_{eh}}{Re}\right) \frac{1 - e^{Re\,\tilde{y}}}{1 - e^{Re}}, \tag{10}$$

where $F_{eh} = h^2(\Delta P + \rho g_x)/\mu$; eq. (10) coincides with the solution derived in [17] when $U_0 = 0$.

Examples of velocity profiles for a given Re and different values of Da are shown in fig. 2 in the case of $U_1 = F_e/2$ (fig. 2(a)) and $U_1 = 1.5\,F_e$ (fig. 2b). Because $\tilde{y}$ lies between 0 and 1, the terms with the hyperbolic sines both tend to decrease as Da increases (*i.e.*, when the permeability decreases for given ϵ and h); the profiles thus become flatter with $\tilde{u}$ being equal to 1 for most of the profile, with higher shear required over increasingly thin boundary layers in order to match the boundary conditions. As shown in fig. 2, the velocities U_0 and U_1 only affect the flow in a small region near the boundaries when $Da = 5000$; large values of Da are common for example in soils, where $\epsilon \sim 0.3$–0.4, h can range from some meters to few hundreds of meters, and κ_x is of the order of $10^{-8}\,\mathrm{m}^2$ even for conductive sands. As Da decreases, the effect of velocity V (*i.e.*, Re), which defines the linearized convective term in eq. (6), becomes more prominent and the maximum value of the velocity moves towards the upper boundary.

3.1.1 Poiseuille flow

A particular case of interest occurs when the flow is horizontal (*i.e.*, $g_x = 0$) and the boundaries are impermeable (*i.e.*, $V = 0$); solutions of this particular case were provided in [20] in 3 dimensions and [9] for zero velocity at the boundaries. We re-call the solution here, giving a physical interpretation in terms of the number Da. When $U_0 = U_1 = 0$, the case is similar to a Poiseuille flow between two solid boundaries that do not move, and the velocity profile from eq. (9) reads

$$u = \frac{\Delta P \kappa_x}{\mu}\left(1 - \frac{e^{(1-y/h)\sqrt{Da}} + e^{y/h\sqrt{Da}}}{1 + e^{\sqrt{Da}}}\right). \tag{11}$$

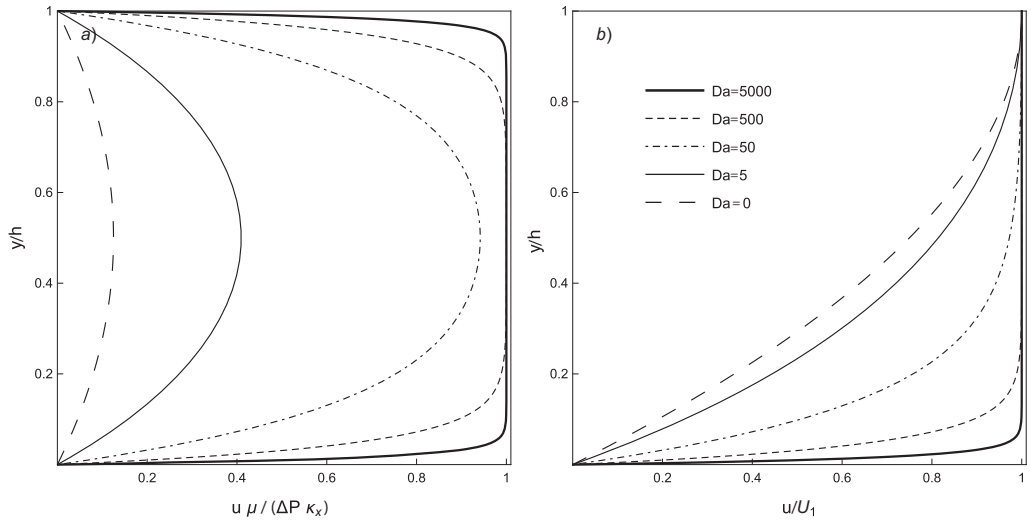

Fig. 3. Examples of velocity profiles for different values of Da as a function of $\tilde{y} = y/h$ for (a) Poiseuille flow (eq. (11)) with $U_0 = U_1 = V = 0$, and (b) free-surface flow (eq. (16)) with $U_0 = V = 0$ and U_1 such that $(\mathrm{d}u/\mathrm{d}y)|_{y=h} = 0$ (eq. (15)).

The maximum velocity, occurring at $y = h/2$, is equal to

$$u_m = \frac{\Delta P \kappa_x}{\mu}\left(1 - \frac{2e^{\sqrt{Da}/2}}{1 + e^{\sqrt{Da}}}\right), \tag{12}$$

and the volumetric flow rate per unit of channel width is

$$Q = \int_0^h u(y)\mathrm{d}y = \frac{\Delta P \kappa_x h}{\mu}\left(1 - \frac{2}{\sqrt{Da}}\tanh(\sqrt{Da}/2)\right). \tag{13}$$

When $\epsilon = 1$ and $\kappa_x \to \infty$, the problem describes the Poiseuille flow with parabolic profile [9,17]

$$u = \frac{\Delta P h^2}{2\mu}\left[\frac{y}{h} - \left(\frac{y}{h}\right)^2\right], \tag{14}$$

and $u_m = \Delta P h^2/(8\mu)$ and $Q = \Delta P h^3/(12\mu)$.

As shown in fig. 3(a), because $V = 0$, the profiles are symmetric with respect to the elevation $y = h/2$, where the maximum velocity occurs. For Da larger than about 100, the maximum velocity, u_m, is only about 1% smaller than $\Delta P \kappa_x/\mu$ (eq. (12)); therefore, when Da becomes larger than 100 the profiles are mostly flat apart from a small region near the boundaries where the velocity is forced to go to zero by the boundary conditions.

3.1.2 Free surface flow

When the flow occurs along a direction at an angle θ to the horizontal, then $g_x = g\sin\theta$. Assuming $\Delta P = 0$, impermeable boundaries (*i.e.*, $V = 0$) and $U_0 = 0$, the additional condition $(\mathrm{d}u/\mathrm{d}y)|_{y=h} = 0$ yields

$$U_1 = \frac{\kappa_x \rho g \sin\theta}{\mu}\left(1 - \frac{2e^{\sqrt{Da}}}{e^{2\sqrt{Da}} + 1}\right). \tag{15}$$

Under these specific conditions, eq. (9) describes the free-surface flow of a film of viscous fluid with thickness h through a porous medium down a plane inclined at an angle θ to the horizontal; this flow is fully driven by gravity along the direction of flow x. The velocity profile in this case reads

$$u = \frac{\rho \kappa_x g \sin\theta}{\mu}\left(1 - \frac{e^{(2-y/h)\sqrt{Da}} + e^{y/h\sqrt{Da}}}{1 + e^{2\sqrt{Da}}}\right), \tag{16}$$

with flow rate

$$Q = \frac{\rho \kappa_x g h \sin\theta}{\mu}\left(1 - \frac{\tanh(\sqrt{Da})}{\sqrt{Da}}\right). \tag{17}$$

When $\epsilon = 1$ and $\kappa_x \to \infty$, eq. (16) becomes [17]

$$u = \frac{\rho g h^2 \sin\theta}{2\mu}\left(2\frac{y}{h} - \left(\frac{y}{h}\right)^2\right), \tag{18}$$

with $U_1 = \rho g h^2 \sin\theta/(2\mu)$ and $Q = \rho g h^3 \sin\theta/(3\mu)$. Equation (18) was used to test a weakly compressible SPH scheme in [26] for open channel flow.

Figure 3(b) shows some examples of velocity profiles for different values of Da. Again, values of Da larger than about 100 generate profiles that are mostly flat with $u = U_1$; as $Da \to 0$, the profile becomes quadratic (eq. (18)) as in open channel flow [26].

3.2 Constant permeability κ_x and non-linear drag

Using the same geometry shown in fig. 1, an exact solution can be found when the resistance to the flow is non-linear, *i.e.* $c_F > 0$ in eq. (4). Assuming that no flow occurs along y (*i.e.*, $V = 0$), and that $u(0) = u(h) = 0$, the equation to be solved for the velocity profile $u(y)$ is

$$\frac{\mathrm{d}^2 u}{\mathrm{d}y^2} - \frac{\epsilon}{\kappa_x}u - \frac{\epsilon \rho c_F}{\mu\sqrt{\kappa_x}}u^2 = -\frac{\epsilon}{\mu}(\Delta P + \rho g_x). \tag{19}$$

This can be re-written as

$$\frac{\mathrm{d}^2 \tilde{u}}{\mathrm{d}\tilde{y}^2} - Da\,\tilde{u} - Da\,A\,\tilde{u}^2 = -Da, \tag{20}$$

where $\tilde{u} = u/F_e = u\mu/[\kappa_x(\Delta P + \rho g_x)]$, $\tilde{y} = y/h$, and $A = F_e \rho c_F \sqrt{\kappa_x}/\mu$. By assuming $q = \mathrm{d}\tilde{u}/\mathrm{d}\tilde{y}$, eq. (20) can be re-written as (see pages 44–47 of [27])

$$q\frac{\mathrm{d}q}{\mathrm{d}\tilde{u}} - Da\,\tilde{u} - Da\,A\,\tilde{u}^2 = -Da, \tag{21}$$

which results into

$$\begin{aligned} q = \frac{\mathrm{d}\tilde{u}}{\mathrm{d}\tilde{y}} &= \pm\sqrt{\frac{-6\,Da\,\tilde{u} + 3\,Da\,\tilde{u}^2 + 2Da\,A\,\tilde{u}^3 + 6DaC_1}{3}} \\ &= \pm\frac{\sqrt{Da}}{\sqrt{3}}\sqrt{-6\tilde{u} + 3\tilde{u}^2 + 2A\tilde{u}^3 + 6C_1}. \end{aligned} \tag{22}$$

Because of the boundary conditions, the velocity profile is expected to be symmetrical with respect to $y = h/2$ (*i.e.*, $\tilde{y} = 1/2$), implying that $q > 0$ when $y < h/2$ (*i.e.*, $\tilde{y} < 1/2$), $q < 0$ when $y > h/2$ (*i.e.*, $\tilde{y} > 1/2$), and $q = 0$ at $y = h/2$ (*i.e.*, $\tilde{y} = 1/2$). Accordingly, u reaches its maximum value, u_m, at $y = h/2$ (*i.e.*, $\tilde{u} = \tilde{u}_m = u_m/F_e$ at $\tilde{y} = 1/2$). This condition leads to

$$C_1 = \tilde{u}_m - \frac{\tilde{u}_m^2}{2} - \frac{\tilde{u}_m^3}{3}A. \tag{23}$$

The profile $\tilde{u}(\tilde{y})$ from the level $\tilde{y} = 0$ to $\tilde{y} < 1/2$ can be thus written as

$$\tilde{y} = \frac{\sqrt{3}}{\sqrt{Da}}\int_0^{\tilde{u}(y)} \frac{\mathrm{d}\hat{u}}{\sqrt{-6d\hat{u} + 3d\hat{u}^2 + 2Ad\hat{u}^3 + 6C_1}}, \tag{24}$$

where $d\hat{u}$ is a dummy variable of integration. Equation (24) also provides a condition to calculate $\tilde{u}_m$ as

$$\frac{1}{2} = \frac{\sqrt{3}}{\sqrt{Da}}\int_0^{\tilde{u}_m} \frac{\mathrm{d}\hat{u}}{\sqrt{-6d\hat{u} + 3d\hat{u}^2 + 2Ad\hat{u}^3 + 6C_1}}. \tag{25}$$

For the solution to exist, the quantity under the root square needs to be positive; therefore, the condition

$$0 < \tilde{u}_m < \frac{\sqrt{4A+1} - 1}{2A} \tag{26}$$

needs to be satisfied.

Figure 4(a) shows examples of the dependence of $\tilde{u}_m$ on Da and ΔP ($g_x = 0$). As Da increases, $\tilde{u}_m$ tends to the limiting value in eq. (26) and the numerical calculation of the integral in eq. (25) becomes difficult to achieve. Figure 4(b) shows the velocity profiles when $Da = 50$ for different values of ΔP.

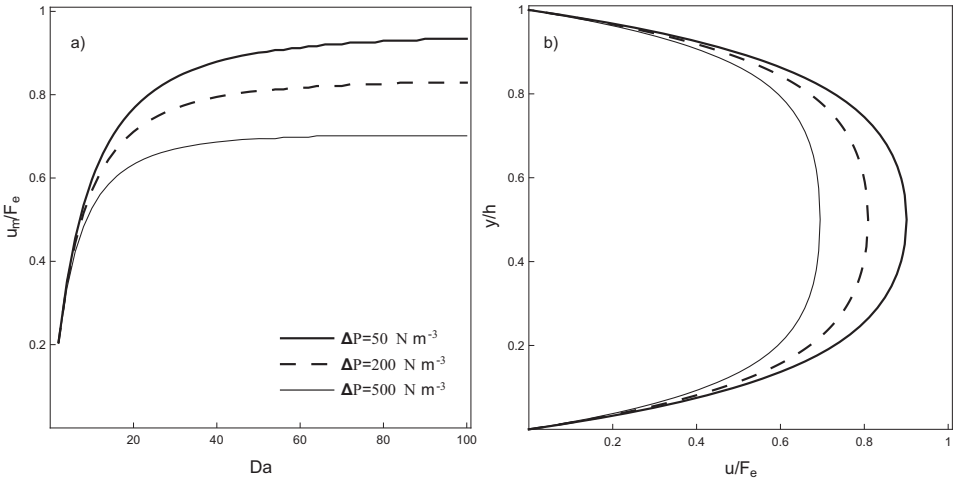

Fig. 4. (a) Examples of $\tilde{u}_m = u_m/F_e$ as a function of Da for different values of ΔP in the case with non-linear drag. (b) Examples of velocity profiles when $Da = 50$ for different values of ΔP as a function of y/h. Other parameters are: $\epsilon = 0.2$, $\kappa_x = 10^{-2}\,\mathrm{m}^2$, $\mu = 1.14\,\mathrm{N\,s\,m}^{-2}$, $\rho = 1260\,\mathrm{kg\,m}^3$, $c_F = 1.2$, $g_x = 0$.

3.3 Spatially varying permeability

In this section we relax the requirement for uniform κ_x. Solutions derived in sect. 3.1 are extended by allowing κ_x to vary as a function of y. In particular we consider two cases: one in which the porous medium consists of a series of stratified horizontal layers of different permeability, and one in which the permeability κ_x changes linearly with y.

3.3.1 Stratified medium

It is assumed that two parallel layers of media with the same porosity, ϵ, and different permeability along x, κ_1 and κ_2, lie one above the other. The two layers are bounded between two plane parallel boundaries, one at the bottom of the first layer and one at the top of the second layer; the two boundaries can be permeable, such that a velocity $v = V$ can be imposed perpendicularly to the main flow direction. The layer at the bottom has a thickness h_1 and the top layer has a thickness h_2. The flow in each of the two layers is driven by a constant pressure gradient along x, $\partial_x p_i = -\Delta P_i$. The longitudinal velocities of the fluid at the two boundaries, U_0 and U_2, are known and provide the boundary conditions of the problem.

Assuming that

$$\begin{aligned} \tilde{y_1} &= \frac{y}{h_1}\,, \quad \text{for } 0 \le y \le h_1, \\ \tilde{y_2} &= \frac{y - h_1}{h_2}\,, \quad \text{for } h_1 \le y \le h_1 + h_2, \end{aligned} \tag{27}$$

the velocity profiles for each layer can be written using eq. (9) as

$$\begin{aligned} u_1(\tilde{y_1}) &= F_{e1}\left[1 + \left(\frac{U_0}{F_{e1}} - 1\right) e^{Re_1\,\tilde{y_1}/2}\frac{\sinh(\sqrt{\alpha_1}(1-\tilde{y_1}))}{\sinh(\sqrt{\alpha_1})} + \left(\frac{U_1}{F_{e1}} - 1\right) e^{-Re_1(1-\tilde{y_1})/2}\frac{\sinh(\sqrt{\alpha_1}\tilde{y_1})}{\sinh(\sqrt{\alpha_1})}\right], \\ u_2(\tilde{y_2}) &= F_{e2}\left[1 + \left(\frac{U_1}{F_{e2}} - 1\right) e^{Re_2\,\tilde{y_2}/2}\frac{\sinh(\sqrt{\alpha_2}(1-\tilde{y_2}))}{\sinh(\sqrt{\alpha_2})} + \left(\frac{U_2}{F_{e2}} - 1\right) e^{-Re_2(1-\tilde{y_2})/2}\frac{\sinh(\sqrt{\alpha_2}\tilde{y_2})}{\sinh(\sqrt{\alpha_2})}\right], \end{aligned}$$

where $F_{ei} = \kappa_i(\Delta P_i + \rho g_x)/\mu$, and $Re_1/Re_2 = h_1/h_2$, because V is the same across the two layers; the Darcy numbers in the two layers are also related through $Da_1/Da_2 = h_1^2\kappa_2/(h_2^2\kappa_1)$. The velocity at the interface between the two layers, U_1, is unknown and can be found by imposing the condition that the shear stress at the interface is the same for the fluid in the two media; this condition means that $d_y u_1(y) = d_y u_2(y)$ for $y = h_1$, and in terms of $\tilde{y_1}$ and $\tilde{y_2}$ becomes

$$\frac{1}{h_1}\left.\frac{\mathrm{d}u_1}{\mathrm{d}\tilde{y_1}}\right|_{\tilde{y}_1=1} = \frac{1}{h_2}\left.\frac{\mathrm{d}u_2}{\mathrm{d}\tilde{y_2}}\right|_{\tilde{y}_2=0}. \tag{28}$$

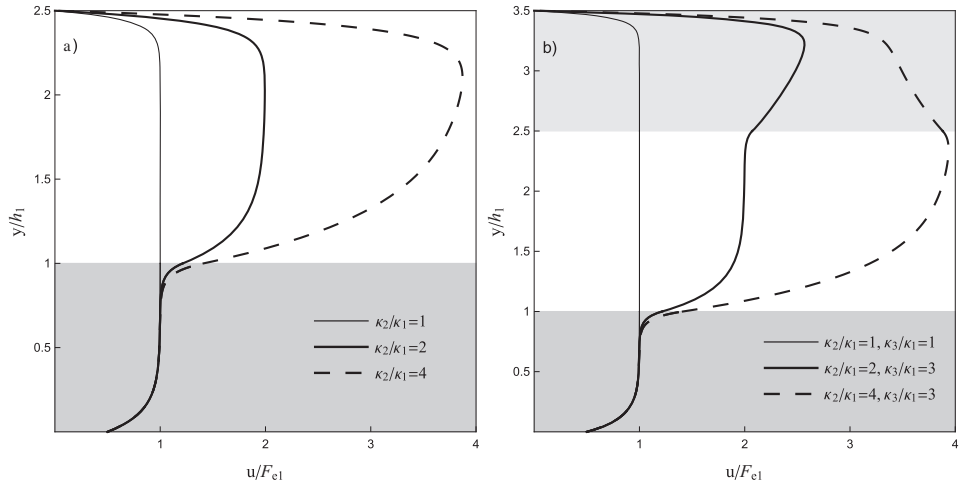

Fig. 5. (a) Velocity profiles in media of different permeability stratified in two layers with $h_2 = 1.5h_1$ and $\Delta P_1 = \Delta P_2$; parameters are $U_0 = F_{e1}/2$, $U_2 = 0$, $Re_1 = 10$, and $Da_1 = 150$. (b) Velocity profiles in three layers with $h_2 = 1.5h_1$, $h_3 = h_1$, and $\Delta P_1 = \Delta P_2 = \Delta P_3$; parameters are $U_0 = F_{e1}/2$, $U_3 = 0$, $Re_1 = 10$, and $Da_1 = 150$.

The velocity U_1 can be shown to be given by

$$\begin{aligned} U_1 = {} & F_{e1}\frac{h_2(2\sqrt{\alpha_1}\coth(\sqrt{\alpha_1}) - 2\sqrt{\alpha_1}e^{Re_1/2}\operatorname{csch}(\sqrt{\alpha_1}) + Re_1)}{2\sqrt{\alpha_2}h_1\coth(\sqrt{\alpha_2}) + 2\sqrt{\alpha_1}h_2\coth(\sqrt{\alpha_1})} \\ & + F_{e2}\frac{h_1(2\sqrt{\alpha_2}\coth(\sqrt{\alpha_2}) - 2\sqrt{\alpha_2}e^{-Re_2/2}\operatorname{csch}(\sqrt{\alpha_2}) - Re_2)}{2\sqrt{\alpha_2}h_1\coth(\sqrt{\alpha_2}) + 2\sqrt{\alpha_1}h_2\coth(\sqrt{\alpha_1})} \\ & + \frac{2\sqrt{\alpha_2}h_1e^{-Re_2/2}U_2\operatorname{csch}(\sqrt{\alpha_2}) + 2\sqrt{\alpha_1}h_2e^{Re_1/2}U_0\operatorname{csch}(\sqrt{\alpha_1})}{2\sqrt{\alpha_2}h_1\coth(\sqrt{\alpha_2}) + 2\sqrt{\alpha_1}h_2\coth(\sqrt{\alpha_1})}\,. \end{aligned} \tag{29}$$

Velocity profiles can then be derived for each layer of porous material, as shown in fig. 5(a).

The same procedure can be used when more than two layers are present. Defining for layer i ($i \in N$ and $i \geq 1$) the variable

$$\tilde{y_i} = \frac{y - \sum_{n=1}^{n=i-1} h_n}{h_i}\,, \quad \text{for} \quad \sum_{n=1}^{n=i-1} h_n \leq y \leq \sum_{n=1}^{n=i} h_n, \tag{30}$$

the velocity profile in each layer can be written as in eq. (9), substituting the velocities at the bottom and top of the layer, U_0 and U_1, with U_{i-1} and U_i respectively. The values of Re and Da in each layer are related to each other through the values of layer thickness, h_i, and permeability, κ_{xi}, according to

$$\frac{Re_i}{h_i} = \frac{\rho V}{\mu} \quad \text{and} \quad \frac{\kappa_{xi}Da_i}{h_i^2} = \epsilon. \tag{31}$$

Imposing the conditions

$$\frac{1}{h_i}\left.\frac{\mathrm{d}u_i}{\mathrm{d}\tilde{y_i}}\right|_{\tilde{y}_i=1} = \frac{1}{h_{i+1}}\left.\frac{\mathrm{d}u_{i+1}}{\mathrm{d}\tilde{y}_{i+1}}\right|_{\tilde{y}_{i+1}=0} \tag{32}$$

at the interface between each layer generates a system of algebraic equations that can be solved to find the velocities at the interface of different layers. Figure 5(b) shows an example with three layers.

3.3.2 κ_x changing linearly with y

An analytic solution can be found when $V = 0$ and $\kappa_x = \kappa_0(1+\gamma y/h)$, with γ a constant parameter. To avoid negative (and unphysical) values of permeability, $\gamma > -1$. When $\gamma = 0$, the problem is described by eq. (6) with $V = 0$. The equation to be solved is

$$\frac{\mathrm{d}^2u}{\mathrm{d}y^2} - \frac{\epsilon}{\kappa_0(1+\gamma y/h)}u = -\frac{\epsilon}{\mu}(\Delta P + \rho g_x). \tag{33}$$

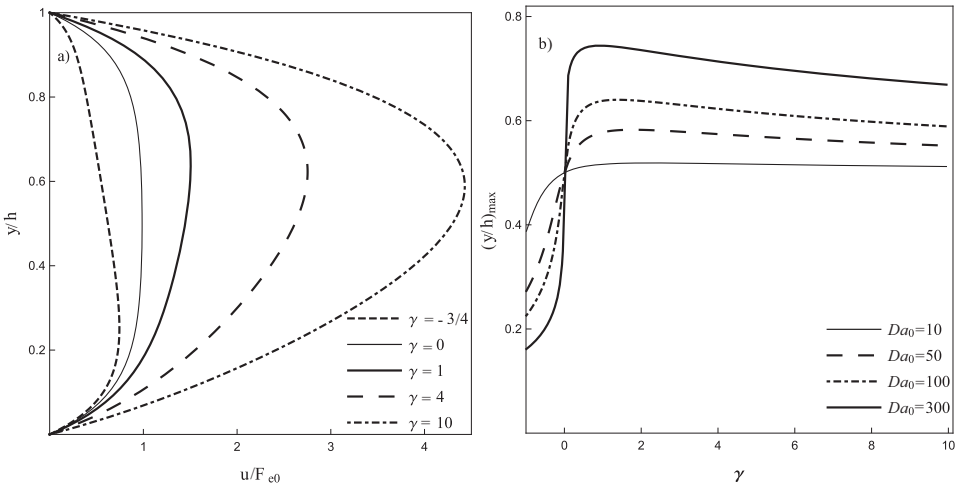

Fig. 6. (a) Velocity profiles when $\kappa_x = \kappa_0(1 + \gamma y/h)$ with $Da_0 = 100$ for different values of γ. (b) Position of the maximum velocity ($(y/h)_{\max}$) as a function of γ for different values of Da_0; note that the minimum value of the horizontal axis is $\gamma = -1$. The boundary conditions are $U_0 = U_1 = V = 0$.

The solution of eq. (33) can be written as (see appendix B)

$$\tilde{u} = C_1 \eta\, I_1(\eta) + C_2 \eta\, K_1(\eta) + \frac{\gamma^2}{4Da_0}\eta^2, \tag{34}$$

where $\tilde{u} = u/F_{e0}$, with $F_{e0} = \kappa_0(\Delta P + \rho g_x)/\mu$, $I_1(\cdot)$ and $K_1(\cdot)$ are the modified Bessel functions of the first and second kind respectively [28], $Da_0 = h^2\epsilon/\kappa_0$, and $\eta = 2\sqrt{Da_0(\tilde{y} + 1/\gamma)/\gamma}$. The two constants C_1 and C_2 can be calculated by imposing the boundary conditions in eq. (5) with $V = 0$; the expressions of these constants are reported in appendix B (see eq. (B.10)).

Examples of velocity profiles for different values of γ, with $U_0 = U_1 = 0$, are shown in fig. 6(a). When γ is negative, the permeability decreases with $\tilde{y}$ such that the maximum velocity, $U_{\max}$, is closer to the boundary at the bottom; the profile is symmetric for $\gamma = 0$ and it becomes asymmetric again as $\gamma > 0$. The position of $U_{\max}$ depends on both γ, which defines how the permeability changes along y, as well as Da_0, which depends on the actual value of permeability κ_0 (fig. 6(b)). As Da_0 increases (*i.e.*, κ_0 decreases with given ϵ and h), when γ is close to -1, $U_{\max}$ tends to be closer to the bottom boundary, while, for positive values of γ, $U_{\max}$ tends to move closer to the upper boundary. When γ becomes zero, the profiles become symmetric and $U_{\max}$ is at $h/2$. As $\gamma \to \infty$, the profile becomes parabolic (as in eq. (14) with $\epsilon = 1$) and $U_{\max}$ again tends to occur at $y = h/2$.

3.4 Time-periodic flow

An exact solution of the classic form of the Navier-Stokes equations for a parallel flow with permeable boundaries and a time-periodically changing pressure gradient was derived in [29]. It is assumed that flow is bounded between stationary parallel boundaries (*i.e.*, $U_0 = U_1 = 0$), and, similarly to [29], that the pressure gradient changes as $\partial_x p = -\Delta P_1 + \Delta P_2 \cos(\omega t) = -\Delta P_1 + \Delta P_2 \Re[e^{i\omega t}]$, where $\Re[z]$ indicates the real part of the complex number z.

The problem to be solved thus is

$$\frac{\partial u}{\partial t} + V\frac{\partial u}{\partial y} = \frac{\epsilon \Delta P_1}{\rho} - \frac{\epsilon \Delta P_2 e^{i\omega t}}{\rho} + \frac{\mu}{\rho}\frac{\partial^2 u}{\partial y^2} + \epsilon g_x - \frac{\mu\epsilon}{\rho\kappa_x}u, \tag{35}$$

with boundary conditions $u(0,t) = 0$ and $u(h,t) = 0$. Note that, again, for the continuity equation, v remains constant and thus equal to V.

A general solution of this problem can be found in the form of

$$u(y,t) = u_1(y) + u_f(y,t) = u_1(y) + \Re[u_2(y)e^{i\omega t}], \tag{36}$$

where u_1 is the steady component of u, due to both ΔP_1 and g_x, while $u_f(y,t) = \Re[u_2(y)e^{i\omega t}]$ is the fluctuating component of the velocity due to $\Delta P_2 \Re[e^{i\omega t}]$. Accordingly, u_1 reads as eq. (9) with $U_0 = U_1 = 0$, and u_2 satisfies the equation

$$\frac{\mathrm{d}^2 u_2}{\mathrm{d}y^2} - \frac{\rho V}{\mu}\frac{\mathrm{d}u_2}{\mathrm{d}y} - \left(i\omega\frac{\rho}{\mu} + \frac{\epsilon}{\kappa_x}\right)u_2 = \frac{\epsilon \Delta P_2}{\mu}\,. \tag{37}$$

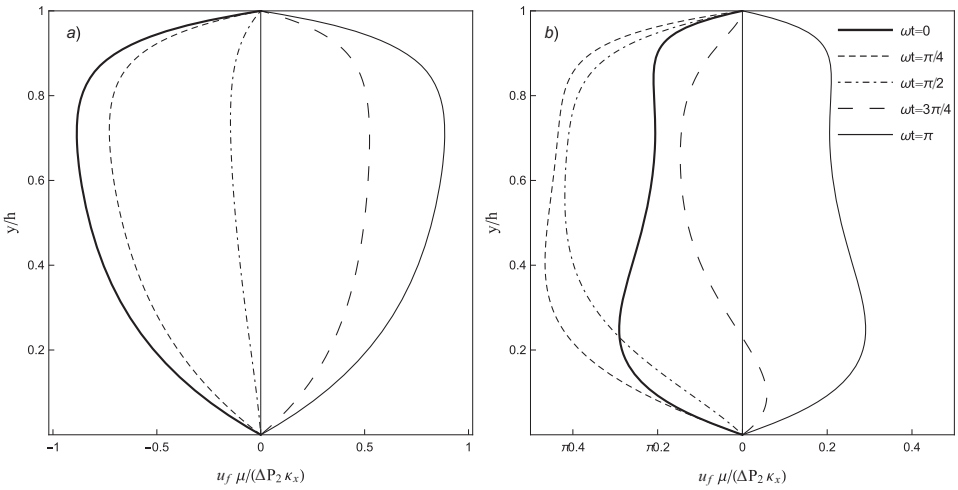

Fig. 7. Magnitude of the velocity profiles, $u_f(y,t)$, for different values of ωt with (a) $M = 10$ and (b) $M = 100$. Other parameters are $Da = 100$ and $Re = 10$.

This equation is similar to eq. (2) and can be solved following the steps in appendix A; u_2 can thus be found as

$$u_2(y) = -\frac{\kappa_x \Delta P_2}{\mu}\frac{Da}{Da+iM}\left[1 - e^{Re\,\tilde{y}/2}\frac{\sinh(\sqrt{\alpha}(1-\tilde{y}))}{\sinh(\sqrt{\alpha})} - e^{-Re(1-\tilde{y})/2}\frac{\sinh(\sqrt{\alpha}\tilde{y})}{\sinh(\sqrt{\alpha})}\right], \tag{38}$$

where $M = \omega\rho h^2/\mu$ is a non-dimensional parameters associated with the frequency of the driving pressure [29] and $\alpha = Re^2/4 + Da + iM$. The oscillating component of the velocity thus reads $u_f(y,t) = \Re[u_2(y)e^{i\omega t}]$. When M is comparable to Re, the profiles of u_f show a single peak along $\tilde{y}$ in time (fig. 7(a)); as M increases two peaks appear along $\tilde{y}$, with the fluctuating component of the velocity having opposite directions (fig. 7(b)).

4 Conclusion

Exact solutions of the two-dimensional generalized Navier-Stokes equations for flow in porous media have been derived for different cases of parallel flow.

When the permeability along the direction of the flow is constant, a general steady-state solution have been obtained accounting for a linearized convection term due to a constant velocity in the direction perpendicular to the main flow. The solutions presented thus extend the existing solutions derived in [9] and [20]. The flow has been found to depend on the Reynolds number associated with the velocity V perpendicular to the flow and the Darcy number dependent on the permeability of the medium. This solution with constant permeability was then used to derive solutions of stratified media. For parallel flow with constant permeability, an exact solution has been derived also when the drag force due to the porous matrix includes a quadratic term of velocity. A case with permeability linearly dependent on the distance from the bottom boundary has been also described and a steady-state solution has been derived in closed form in terms of Bessel functions. Finally, again for the case with constant permeability, an unsteady solution was derived when the pressure gradient driving the flow fluctuates periodically in time. This thus extends the solution by [29] to flows in porous media.

The suite of solutions obtained and presented here can be used as benchmarks for numerical schemes. This appears particularly important in the context of SPH modelling, which still lacks exact solutions for the validation of numerical schemes for flow in porous media.

Aside from providing numerical benchmarks, the applicability of the solution presented in practical problems relies on their stability. As suggested by [30], for small values of porosity and low hydraulic permeability (*i.e.*, large values of Da), flows in porous media can be modeled using the Darcy's law, which is expected to be stable to small perturbations for all Reynold numbers associated with the longitudinal flow [30]. However, as the porosity and the hydraulic permeability increase (*i.e.*, Da decreases), such as in hyper-porous materials, the description of the flow becomes closer to that described by the classic form of the Navier-Stokes equations, with the stability of the flow to small perturbations being dependent on the Reynolds number of the longitudinal flow. Results about the stability of flow to small perturbations are available for, *e.g.*, plane Poiseuille flow (sect. 3.1.1). In the case of the classic Navier-Stokes equations (*i.e.*, $Da \to 0$), the plane Poiseuille flow is stable to small perturbations for values of the Reynolds number ($= u(h/2)/\nu$) lower than the critical value 5772 [30, 31]. As discussed in [30] and [32], the critical values of these Reynolds number increase as Da increases. Readers are directed to [33] for a more general discussion of flow stability in porous media.

Some of the results and figures were obtained using Wolfram Mathematica® 11.2. ED thanks the Faculty of Engineering at Monash University for supporting his Outside Study Program and the Department of Civil, Environmental and Architectural Engineering at the University of Padova, Italy, for hosting him when this study was undertaken.

Appendix A. Derivation of eq. (9)

By introducing the variables

$$u = \tilde{u}\frac{\kappa_x}{\mu}(\Delta P + \rho g_x) = \tilde{u}F_e, \quad y = \tilde{y}h, \tag{A.1}$$

eq. (2) can be written in non-dimensional terms as

$$\frac{\mathrm{d}^2\tilde{u}}{\mathrm{d}\tilde{y}^2} - Re\,\frac{\mathrm{d}\tilde{u}}{\mathrm{d}\tilde{y}} - Da\,\tilde{u} = -Da, \tag{A.2}$$

with $Re = \rho V h/\mu$ and $Da = \epsilon h^2/\kappa_x$. Using the change of variables $\tilde{u} = w(y)\exp[Re\,\tilde{y}/2]$, eq. (A.2) can be modified into

$$\frac{\mathrm{d}^2 w}{\mathrm{d}y^2} - \left(Re^2/4 + Da\right) w = -Da\, e^{-Re\,\tilde{y}/2}, \tag{A.3}$$

the solution of which reads (see eq. (2.1.9.1) of [34])

$$w = C_1\cosh(\sqrt{\alpha}\tilde{y}) + C_2\sinh(\sqrt{\alpha}\tilde{y}) + \mathrm{e}^{-Re\,\tilde{y}/2}, \tag{A.4}$$

where $\alpha = Re^2/4 + Da$. The variable u can then be written as in eq. (9) by imposing the boundary conditions in eq. (5).

Appendix B. Derivation of eq. (34)

By introducing the variables

$$u = \tilde{u}\frac{\kappa_0}{\mu}(\Delta P + \rho g_x) = \tilde{u}F_{e0}, \quad y = \tilde{y}h, \tag{B.1}$$

eq. (33) can be transformed into

$$\frac{\mathrm{d}^2\tilde{u}}{\mathrm{d}\tilde{y}^2} - \frac{Da}{1+\gamma\tilde{y}}\,\tilde{u} = -Da. \tag{B.2}$$

The solution of eq. (B.2) can be formally written as (see sect. 0.2.1-6 of [34])

$$\tilde{u} = C_1 u_{h1} + C_2 u_{h2} - Da\,u_{h2}\int \frac{u_{h1}}{W(\tilde{y})}\,\mathrm{d}\tilde{y} + Da\,u_{h1}\int \frac{u_{h2}}{W(\tilde{y})}\,\mathrm{d}\tilde{y}, \tag{B.3}$$

where $W(\tilde{y}) = u_{h1}(\mathrm{d}u_{h2}/\mathrm{d}\tilde{y}) - u_{h2}(\mathrm{d}u_{h1}/\mathrm{d}\tilde{y})$, and u_{h1} and u_{h2} are independent solutions of the homogeneous equation associated with eq. (B.2); this homogeneous equation can be re-written as

$$\frac{\mathrm{d}^2 u_h}{\mathrm{d}\xi^2} - \frac{Da}{\gamma\xi}u_h = 0, \tag{B.4}$$

with $\xi = \tilde{y} + 1/\gamma$. Solutions of the homogeneous equation can be found as (see eq. (2.1.2.7) of [34])

$$\begin{aligned} u_h(\eta) &= C_1 u_{h1} + C_2 u_{h2} \\ &= C_1\eta I_1(\eta) + C_2\eta K_1(\eta), \end{aligned} \tag{B.5}$$

where $\eta = 2\sqrt{Da\xi/\gamma}$, and $I_1(\cdot)$ and $K_1(\cdot)$ are the modified Bessel functions of the first and second kind, respectively [28]. The function W can be expressed as

$$\begin{aligned} W(\tilde{y}) &= u_{h1}\frac{\mathrm{d}u_{h2}}{\mathrm{d}\tilde{y}} - u_{h2}\frac{\mathrm{d}u_{h1}}{\mathrm{d}\tilde{y}} && \text{(B.6)}\\ &= u_{h1}(\eta)\frac{\mathrm{d}u_{h2}}{\mathrm{d}\eta}\frac{\mathrm{d}\eta}{\mathrm{d}\xi}\frac{\mathrm{d}\xi}{\mathrm{d}\tilde{y}} - u_{h2}(\eta)\frac{\mathrm{d}u_{h1}}{\mathrm{d}\eta}\frac{\mathrm{d}\eta}{\mathrm{d}\xi}\frac{\mathrm{d}\xi}{\mathrm{d}\tilde{y}}\\ &= \frac{\mathrm{d}\eta}{\mathrm{d}\xi}\frac{\mathrm{d}\xi}{\mathrm{d}\tilde{y}}\left[\eta I_1(\eta)(\eta K_1(\eta))' - \eta K_1(\eta)(\eta I_1(\eta))'\right]\\ &= -\frac{\eta^2}{2}\frac{\mathrm{d}\eta}{\mathrm{d}\xi}\frac{\mathrm{d}\xi}{\mathrm{d}\tilde{y}}[I_1(\eta)K_0(\eta) + I_0(\eta)K_1(\eta)] - \frac{\eta^2}{2}\frac{\mathrm{d}\eta}{\mathrm{d}\xi}\frac{\mathrm{d}\xi}{\mathrm{d}\tilde{y}}[I_2(\eta)K_1(\eta) + I_1(\eta)K_2(\eta)] && \text{(B.7)}\\ &= -\frac{\eta^2}{2}\frac{\mathrm{d}\eta}{\mathrm{d}\xi}\frac{\mathrm{d}\xi}{\mathrm{d}\tilde{y}}\frac{2}{\eta} && \text{(B.8)}\\ &= -\eta\frac{\mathrm{d}\eta}{\mathrm{d}\xi}, \end{aligned}$$

where the step (B.7) is obtained using 9.2.26 in [28], the step (B.8) is obtained using 9.6.15 in [28], and the final result derives from $\mathrm{d}\xi = \mathrm{d}\tilde{y}$.

Noticing that

$$\mathrm{d}\tilde{y} = \mathrm{d}\xi = \frac{\gamma}{2Da}\eta\mathrm{d}\eta, \tag{B.9}$$

the first integral term in eq. (B.3) can be written as

$$\begin{aligned} -Da\,u_{h2}\int\frac{u_{h1}}{W(\tilde{y})}\mathrm{d}\tilde{y} &= +Da\,u_{h2}\int\frac{\eta\,I_1(\eta)}{\eta}\frac{\mathrm{d}\xi}{\mathrm{d}\eta}\mathrm{d}\tilde{y}\\ &= Da\,u_{h2}\int I_1(\eta)\left(\frac{\mathrm{d}\xi}{\mathrm{d}\eta}\right)^2\mathrm{d}\eta\\ &= Da\,u_{h2}\int I_1(\eta)\left(\frac{\gamma}{2Da}\eta\right)^2\mathrm{d}\eta\\ &= \frac{\gamma^2}{4Da}u_{h2}\int\eta^2 I_1(\eta)\mathrm{d}\eta\\ &= \frac{\gamma^2}{4Da}u_{h2}\eta^2 I_2(\eta) = \frac{\gamma^2}{4Da}\eta^3 K_1(\eta)I_2(\eta), \end{aligned}$$

where the last integration is obtained from 11.3 of [28]. Following similar steps, the second integration of eq. (B.3) is

$$\begin{aligned} Da\,u_{h1}\int\frac{u_{h2}}{W(\tilde{y})}\mathrm{d}\tilde{y} &= -Da\,u_{h1}\int K_1(\eta)\left(\frac{\gamma}{2Da}\eta\right)^2\mathrm{d}\eta\\ &= -\frac{\gamma^2}{4Da}u_{h1}\int\eta^2 K_1(\eta)\mathrm{d}\eta\\ &= +\frac{\gamma^2}{4Da}u_{h1}\eta^2 K_2(\eta) = \frac{\gamma^2}{4Da}\eta^3 I_1(\eta)K_2(\eta). \end{aligned}$$

The sum of the two integrals results to be

$$-Da\,u_{h2}\int\frac{u_{h1}}{W(\tilde{y})}\mathrm{d}\tilde{y} + Da\,u_{h1}\int\frac{u_{h2}}{W(\tilde{y})}\mathrm{d}\tilde{y} = \frac{\gamma^2}{4Da}\eta^3[I_1(\eta)K_2(\eta) + K_1(\eta)I_2(\eta)] = \frac{\gamma^2}{4Da}\eta^2,$$

where the last equality is again obtained using 9.6.15 of [28]. The solution of eq. (B.2) can then be written as eq. (34).

The two constants C_1 and C_2 in eq. (34) can be obtained by imposing the conditions

$$\begin{aligned} &\tilde{u} = U_0, \quad \text{for } \tilde{y} = 0, \eta = \eta_0 = 2\sqrt{Da}/\gamma,\\ &\tilde{u} = U_1, \quad \text{for } \tilde{y} = 1, \eta = \eta_1 = 2\sqrt{Da(\gamma+1)}/\gamma, \end{aligned}$$

which lead to

$$C_1 = \frac{(\gamma+1-U_1)\eta_0 K_1(\eta_0) - (1-U_0)\eta_1 K_1(\eta_1)}{\eta_0\eta_1[I_1(\eta_0)K_1(\eta_1) - I_1(\eta_1)K_1(\eta_0)]},$$
$$C_2 = \frac{-(\gamma+1-U_1)\eta_0 I_1(\eta_0) + (1-U_0)\eta_1 I_1(\eta_1)}{\eta_0\eta_1[I_1(\eta_0)K_1(\eta_1) - I_1(\eta_1)K_1(\eta_0)]}. \tag{B.10}$$

In the case $U_0 = U_1 = 0$, the two constants of integration are

$$C_1 = \frac{(\gamma+1)\eta_0 K_1(\eta_0) - \eta_1 K_1(\eta_1)}{\eta_0\eta_1[I_1(\eta_0)K_1(\eta_1) - I_1(\eta_1)K_1(\eta_0)]}$$
$$C_2 = \frac{-(\gamma+1)\eta_0 I_1(\eta_0) + \eta_1 I_1(\eta_1)}{\eta_0\eta_1[I_1(\eta_0)K_1(\eta_1) - I_1(\eta_1)K_1(\eta_0)]}. \tag{B.11}$$

References

1. J. Bear, *Dynamics of Fluids in Porous Media* (Elsevier, Amsterdam, 1972).
2. P.Y. Polubarinova-Kochina, *Theory of Groundwater Movement* (Princeton University Press, Princeton, N.J., 1962).
3. D.A. Nield, A. Bejan, *Convection in Porous Media* (Springer, Cham, 2017).
4. K.G. Boggs, R.W. Van Kirk, G.S. Johnson, J.P. Fairley, P.S. Porter, J. Am. Water Resour. Assoc. **46**, 1116 (2010).
5. Peter Troch, Emiel van Loon, Arno Hilberts, Adv. Water Resour. **25**, 637 (2002).
6. E. Daly, A. Porporato, Phys. Rev. E **70**, 056303 (2004).
7. E. Daly, A. Porporato, Water Resour. Res. **40**, W016011 (2004).
8. M.S. Bartlett, A. Porporato, Water Resour. Res. **54**, 767 (2018).
9. M.H. Hamdan, Appl. Math. Comput. **62**, 203 (1994).
10. H.C. Brinkman, Appl. Sci. Res. **A1**, 27 (1947).
11. B. Goyeau, D. Lhuillier, D. Gobin, M.G. Velarde, Int. J. Heat Mass Transfer **46**, 4071 (2003).
12. F.J. Valds-Parada, C.G. Aguilar-Madera, J.A. Ochoa-Tapia, B. Goyeau, Adv. Water Resour. **62**, 327 (2013).
13. H. Akbari, M.M. Namin, Coast. Eng. **74**, 59 (2013).
14. H. Akbari, Coast. Eng. **89**, 1 (2014).
15. H. Basser, M. Rudman, E. Daly, Adv. Water Resour. **108**, 15 (2017).
16. J.J. Monaghan, Annu. Rev. Fluid Mech. **44**, 323 (2012).
17. P.G. Drazin, N. Riley, *The Navier-Stokes equations: A classification of flows and exact solutions*, in *London Mathematical Society Lecture Notes Series* (Cambridge University Press, Cambridge, 2006).
18. C.Y. Wang, Appl. Mech. Rev. **42**, S269 (1989).
19. C.Y. Wang, Annu. Rev. Fluid Mech. **23**, 159 (1991).
20. A. Bourchtein, Int. J. Numer. Methods Fluids **39**, 1053 (2002).
21. W. Khan, F. Yousafzai, M. Ikhlaq Chohan, A. Zeb, G. Zaman, I.H. Jung, Int. J. Pure Appl. Math. **96**, 235 (2014).
22. C. Beckermann, R. Viskanta, S. Ramadhyani, J. Fluid Mech. **186**, 257 (2006).
23. C. Beckermann, S. Ramadhyani, R. Viskanta, J. Heat Transf. **109**, 363 (1987).
24. D.D. Joseph, D.A. Nield, G. Papanicolaou, Water Resour. Res. **18**, 1049 (1982).
25. D.A. Nield, Transp. Porous Media **78**, 537 (2009).
26. I. Federico, S. Marrone, A. Colagrossi, F. Aristodemo, M. Antuono, Eur. J. Mech. B/Fluids **34**, 35 (2012).
27. W.F. Ames, *Nonlinear Ordinary Differential Equations in Transport Processes* (Academic Press, New York, 1968).
28. M. Abramowitz, I.A. Stegun, *Handbook of Mathematical Functions* (Dover, New York, 1965).
29. C.Y. Wang, J. Appl. Mech. **38**, 553 (1971).
30. D.A. Nield, Int. J. Heat Mass Transfer **46**, 4351 (2003).
31. P.G. Drazin, W.G. Reid, *Hydrodynamic Stability*, 2nd ed. (Cambridge University Press, Cambridge, 2004).
32. Antony A. Hill, Brian Straughan, *Stability of Poiseuille flow in a porous medium* (Springer, Berlin, Heidelberg, 2010) pp. 287–293.
33. B. Straughan, *Stability and wave motion in porous media*, in *Applied Mathematical Sciences* (Springer, New York, 2008).
34. A.D. Polyanin, V.F. Zaitsev, *Handbook of Exact Solutions for Ordinary Differential Equations* (CRC Press, Boca Raton, 2003).